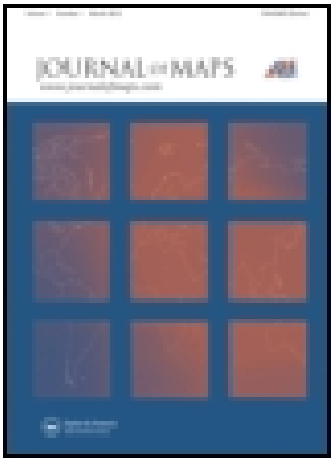

Journal of Maps
Publication details, including instructions for authors and subscription information:
http://www.tandfonline.com/loi/tjom20

Weathering grade and geotectonics of the western-central Mucone River basin (Calabria, Italy)

Luigi Borrelli[a], Salvatore Critelli[b], Giovanni Gullà[a] & Francesco Muto[b]

[a] CNR-IRPI, Via Cavour 4/6, 87030 Rende (CS), Italy

[b] Dipartimento di Biologia, Università della Calabria, Ecologia e Scienze della Terra, 87036 Arcavacata di Rende (CS), Italy

Published online: 03 Jul 2014.

To cite this article: Luigi Borrelli, Salvatore Critelli, Giovanni Gullà & Francesco Muto (2014): Weathering grade and geotectonics of the western-central Mucone River basin (Calabria, Italy), Journal of Maps, DOI: 10.1080/17445647.2014.933719

To link to this article: http://dx.doi.org/10.1080/17445647.2014.933719

Journal of Maps, 2014
http://dx.doi.org/10.1080/17445647.2014.933719

SCIENCE

Weathering grade and geotectonics of the western-central Mucone River basin (Calabria, Italy)

Luigi Borrelli[a*], Salvatore Critelli[b], Giovanni Gullà[a] and Francesco Muto[b]

[a]*CNR-IRPI, Via Cavour 4/6, 87030 Rende (CS), Italy;* [b]*Dipartimento di Biologia, Università della Calabria, Ecologia e Scienze della Terra, 87036 Arcavacata di Rende (CS), Italy*

(*Received 10 March 2014; resubmitted 22 May 2014; accepted 9 June 2014*)

This paper illustrates the compilation of an engineering geological map based on structural architecture and weathering grade of crystalline rocks occurring in the central-western portions of the Mucone River basin (Sila Massif, Calabria, Italy). The map, drawn at 1:10,000 scale and covering an area of about 100 km^2, was compiled by combining new geological and structural data with the results of a weathering-grade field survey. Five weathering classes, each characterized by comparable mechanical behaviour, have been mapped, from the class VI (residual and colluvial soils) to class II (slightly weathered rock). Both qualitative and semi-quantitative criteria (e.g. rock colour, discolouration processes, samples broken by hand and hammer, sound of the rock when it is struck by a geological hammer, Schmidt Hammer tests) were used to distinguish and map weathering-grade classes at outcrop scale.

The thematic map presented in this paper aims to provide a useful tool for land planning policy, for the evaluation of geological and geotechnical hazard and for environmental and engineering perspectives of land use.

Keywords: crystalline rocks; weathering-grade map; engineering geology purpose; Calabria; southern Italy

1. Introduction

Geo-engineering thematic maps are a useful tools for territorial planning and management (Bell & Pettinga, 1985; Conforti, Muto, Rago, & Critelli, 2014; Dearman, 1974, 1991; Dearman & Eyles, 1982; Dearman & Matula, 1976; Faccini, Robbiano, Roccati, & Angelini, 2012; Grman, Waniekova, Petro, & Polascinova, 2002; IAEG, 1976; Lozinska-Stepien, 1979; Maharaj, 1995; Zuquette, Pejon, & dos Santos Collares, 2004). Focussing on the production of specific geo-engineering maps, where the subject is the subdivision of weathering intensity of crystalline rocks, it is important to define, classify and map the weathering grade for outcrops (Borrelli, Greco, & Gullà, 2007; Calcaterra & Parise, 2005; Cascini, Critelli, Di Nocera, Gullà, & Matano, 1992; GSEGWP, 1995; Malomo, Olorunniwo, & Ogunsanwo, 1983). In fact, a thematic map which provides the distinction of different weathering classes, each of which is characterized

*Corresponding author. Email: l.borrelli@irpi.cnr.it

by comparable mechanical behaviour, may be useful for many purposes: engineering geology, environmental geology, and land-use.

Based on the principle that the weathering grade of outcropping crystalline rocks reflects their engineering characteristics and performance (Baynes, Dearman, & Irfan, 1978; Dearman & Matula, 1976; GCO, 1988; IAEG, 1981; Irfan & Dearman, 1978), in this paper we focus on the subdivision and mapping of weathering grade, through observation of distinctive geological characteristics and qualitative and semi-quantitative engineering geological tests (Borrelli et al., 2007; Gullà & Matano, 1997).

The weathering-grade map was produced for a large area (about 100 km^2), located in the west-central side of the Mucone River basin, close to the Acri Village (northern Calabria,

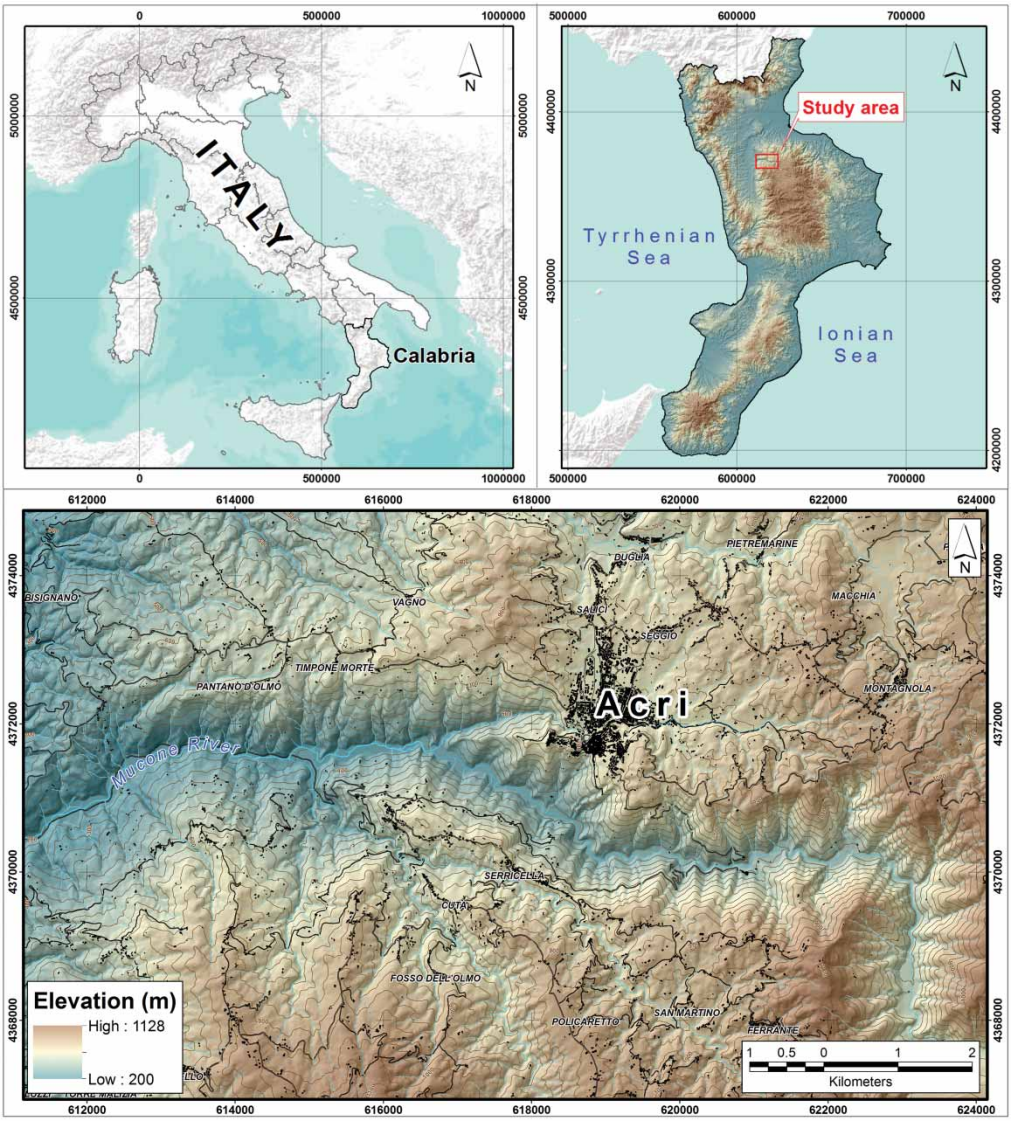

Figure 1. Location of the study area.

Italy) (Figure 1). The map reflects the effects of weathering in an area characterized by active tectonics and rapid landscape evolution (e.g. intense denudation processes), providing a fundamental contribution to the assessment of landslide and soil erosion hazards.

2. Geological framework of the Sila Massif

The study area is located on the north-western slope of the Sila Massif (northern Calabria) (Figure 2). The Sila Massif is one of the key zones of the Calabrian terranes (Critelli, Muto,

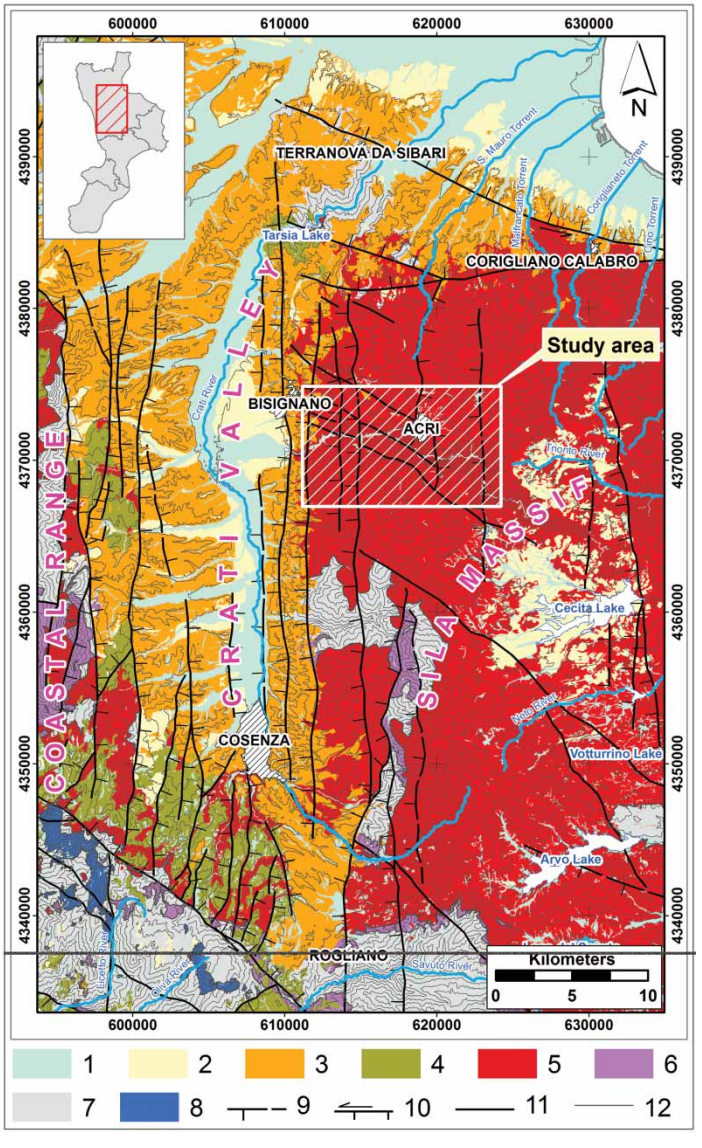

Figure 2. Geo-structural sketch of study sector. Legend: (1) Holocene deposits; (2) Upper Pleistocene deposits; (3) Pliocene-Middle Pleistocene deposits; (4) Upper-Middle Miocene deposits; (5) Sila Unit (Paleozoic); (6) Castagna Unit (Paleozoic); (7) Slate-metapelite and ophiolitic Units (Paleozoic-Mesozoic); (8) Monte Cocuzzo Unit (Mesozoic); (9) normal fault; (10) left-lateral transtensive fault; (11) fault with undetermined kinematics; and (12) tectonic contact.

Tripodi, & Perri, 2013; Messina et al., 1994; Van Dijk et al., 2000). Its structure has been formed since the Late Oligocene-early Miocene, in response to accrectionary processes towards the Adriatic foreland and since the Tortonian became a morphostructural high having an elevation similar to the present day (Critelli et al., 2013). The uppermost crystalline nappe of the Calabrian Arc tectonic edifice is made up of Paleozoic metamorphic (from low-to-high-grade rocks) and plutonic rocks included in the Sila Unit (Messina et al., 1994) and widely outcropping along the entire Sila Massif (Figure 2).

Since the Late Miocene, the Sila Massif experienced brittle deformation that fragmented the pre-Pliocene rocks in a series of horst and graben structures (e.g. Sila Massif and Coastal Range, Figure 2; Barone, Dominici, Muto, & Critelli, 2008; Spina, Tondi, & Mazzoli, 2011). Since the Early Pleistocene, following the extensional tectonic phase of the Calabrian Arc, a huge clastic supply (conglomerate, sand and mud), has progressively filled the Crati Basin and sourrounding basins (Fabbricatore, Robustelli, & Muto, 2014; Perri et al., 2012; Perri, Borrelli, Gullà, & Critelli, 2014; Spina et al., 2011).

From a tectonic perspective, the Sila Massif is characterized by a structural style mainly dominated by the intersection of regional fault systems trending N-S and NW-SE, respectively (Figure 2) (Spina et al., 2011; Van Dijk et al., 2000).

The N-S fault system developed as normal system during the Middle Pleistocene in response to abrupt regional tectonic uplift; the system shows present day activity as testified by intense seismicity along the western and eastern piedmont zone of the Sila Massif (Spina et al., 2011; Tortorici, Monaco, Tansi, & Cocina, 1995).

The NW-SE fault system is characterized by inherited and reactivated pre-existing early Pleistocene regional left strike slip faults well developed at the boundary between the Apennine and the Calabrian Arc (Van Dijk et al., 2000 and references therein). During the last extensional tectonic phase of the Late Pleistocene, the NW-SE faults were reactivated (Corbi et al., 2009; Lanzafame & Tortorici, 1981; Tansi, Muto, Critelli, & Iovine, 2007).

Since the late Miocene, the basement rocks of the Sila Massif experienced intense weathering processes resulting in deep weathering profiles, weathered landforms and abrupt erosional processes removing portions of the deeply weathered rocks (e.g. Borrelli, Perri, Critelli, & Gullà, 2014; Guzzetta, 1974; Matano & Di Nocera, 1999). The intense erosion activated by Pleistocene uplift has prevailed over weathering processes, although not enough to completely remove the exposed, deeply weathered mantle (e.g. Calcaterra & Parise, 2010; Garfi, Bruno, Calcaterra, & Parise, 2007; Le Pera, Arribas, Critelli, & Tortosa, 2001a; Le Pera, Critelli, & Sorriso-Valvo, 2001b; Matano & Di Nocera, 1999; Molin, Pazzaglia, & Dramis, 2004; Scarciglia, Le Pera, & Critelli, 2005a, 2007; Scarciglia, Le Pera, Vecchio, & Critelli, 2005b).

3. Methods

Geological survey maps were used as a preliminary basis for rock type identification in the study area. The outcropping crystalline rock type and, in particular, the high-grade metamorphic rocks, were identified on the basis of typical distinctive characteristics (e.g. structure, foliation, mineralogical composition), and with the additional help of petrographic evidence (Borrelli, 2008).

Aerial photo interpretation based on identification of the main Quaternary features was performed to identify key morphological evidence related to tectonics; field control was made to confirm the features identified on aerial photographs. The kinematic characterization of the

surveyed faults and the areal meso-structural analysis (on over 80 structural stations) was carried out to verify typology and chronology of tectonic deformation.

With regard to the surveying of weathering grade, the procedure was divided in three phases (Figure 3): (1) photo-interpretative analysis; (2) weathering surveys; and (3) analysis of the collected data and production of the weathering grade map.

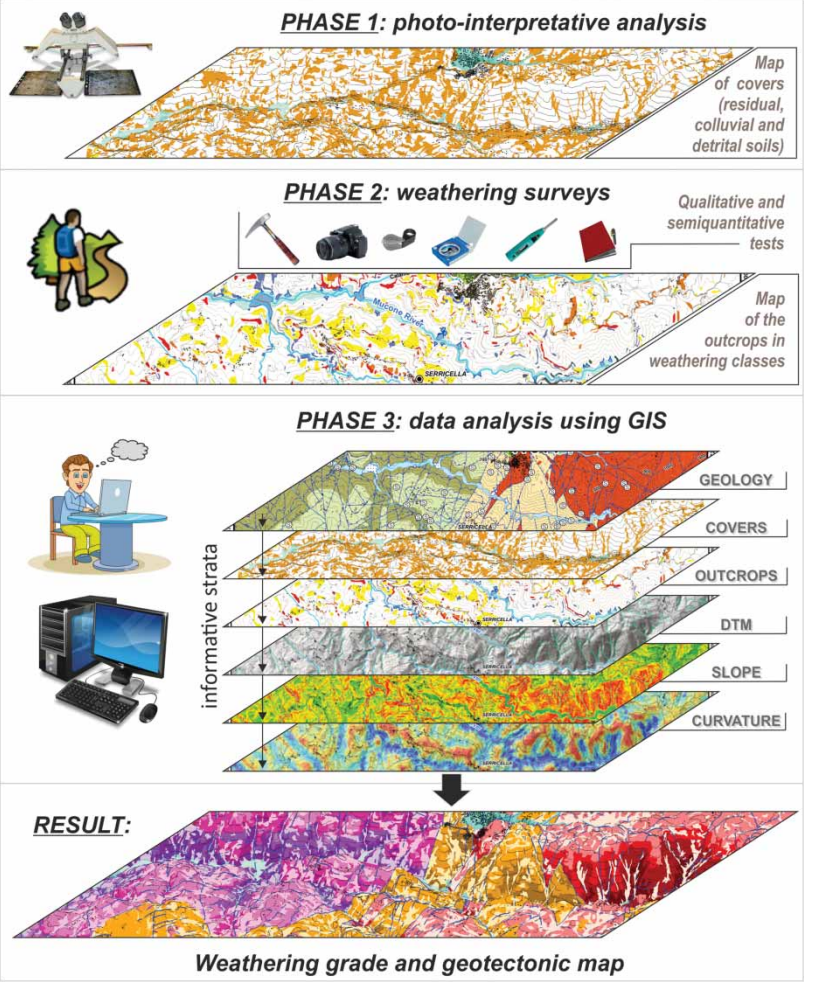

Figure 3. Schematic of the methodological approach used for the production of the weathering-grade map.

Through photo-interpretative analysis of two series of black and white panchromatic air photos, dating to 1955 and 1991 (Italian Military Geographical Institute), we identified, for the plutonic and metamorphic rocks, two macro-classes of weathering (Borrelli, Cofone, & Gullà, 2012a): areas where there are soils formed by in-situ weathering (residual soils) and transported soils (colluvial and detrital soils); areas where crystalline bedrock outcrops occur (with typical mechanical behaviour of weak or hard-rock). The main geo-environmental features used in this

preliminary analysis were slope angle, relief contour and land use. In most cases, macro-classes were defined on the basis of the landscape evidence (i.e. paleosurfaces, morphology, slope angle, etc.). This analysis was followed by the field weathering survey along road cuts, river valleys and exposed sections to verify the features identified on aerial photographs.

The field weathering survey (1:10,000 scale) required the definition of specific codified procedures to allow the identification of different classes of weathering at outcrop scale. The criteria, simplified for large areas, were suggested by GCO (1988), Cascini et al. (1992), GSE-GWPR (1995), Gullà and Matano (1997), Borrelli et al. (2007), and Borrelli (2008), that subdivide the grade into six weathering classes: class VI (residual and colluvial soils and detrital weathered material); class V (completely weathered rock); class IV (highly weathered rock); class III (moderately weathered rock); class II (slightly weathered rock); class I (fresh rock).

During the weathering field surveys, the main engineering geological features of the different classes were obtained through visual recognition of mineral alteration, rock and soil ratios, the presence of original texture and structure, joint staining, degree of discolouration, and by means of a number of simple index tests by using the geological hammer. In particular, rapid identification, the strength was assessed by geological hammer (e.g. sound emitted from the rock when is struck with the hammer, hammer head effect, hammer point effect, hammer breaking), and trying to break the rock fragments by hand (length about 15 cm).

Usually, the fresh to slightly weathered rock remains intact or exhibits slight modifications and produces a ringing sound when it is struck by a geological hammer; the moderately weathered rock produces a ringing to intermediate sound when it is struck by a hammer, whereas highly weathered rock produces an intermediate sound and large pieces of rocks are broken by hand; a dull sound is produced from soil-like rock (completely weathered rocks and residual soils), which can be easily crumbled by hand or finger pressure.

In uncertain cases, tests with the Schmidt Hammer were carried out using the criteria of Gullà and Matano (1997), to determine the weathering classes. In addition, micropetrographic and microfracture indexes were used to supplement and to refine the field classification (Borrelli, Perri, Critelli, & Gullà, 2012b; Borrelli et al., 2014).

Overall analysis and management of the data was undertaken using a geographical information system (GIS) supplemented with a digital terrain model (DTM 10 m $\times$ 10 m, interpolated from the contour lines and points of the 1:10,000 scale topographic maps), slope map and curvature map (produced from the DTM). In particular, terrain attributes (such as relief, slope, curvature) were used to extend the weathering mapping to areas not covered by the field survey, based on the assumption that where there are high slope angles or convex curvature, slightly to highly weathered rocks are present. In contrast, in low relief landscapes weathered rocks or residual soils are completely preserved. Finally, where concave curvature occurs, thin or thick colluvial and detritical soils are present.

4. Weathering grade and geotectonic map

In the study area three main morphological sectors can be distinguished: summit surfaces, slopes, and the valley. Summit surfaces represent the remnants of an ancient low relief landscape almost totally removed by erosion. The slopes are characterized by high gradient values (30°–40°) and deep incisions down to the crystalline basement, where erosion and mass movements are widely present (Borrelli et al., 2007). The valley is mostly characterized by sedimentation (e.g. alluvial debris flow fan and detrital fan), with local alternating erosional processes.

The Palaeozoic crystalline lithologies, outcropping in the study area, mainly represented by the Sila Unit (Messina et al., 1994), include medium-to-high-grade metamorphic and granitoid rocks.

Based on field observations and petrographic evidence in thin-sections (Borrelli, 2008), metamorphic rocks have been distinguished into, (a) biotite-garnet-sillimanite gneiss, (b) biotite-sillimanite migmatitic gneiss, and (c) biotite-muscovite migmatitic gneiss (Figure 4).

Biotite-rich and garnet-sillimanite gneisses occur dominantly in the central and western portions of the study area (Figure 4). They are present in correspondence with the middle-and-lower slopes (from 200 m to 600 m a.s.l.) of the main fluvial channels of the Mucone River and Ceraco, Braso and Calamo torrents (Figure 4). At the outcrop scale, these rocks are dark, reddish to purple in colour, variously schistose to massive (Figure 5(a)) and characterized by an intense weathering profile (e.g. Borrelli et al., 2012a, 2014; Le Pera et al., 2001a, 2001b; Scarciglia et al., 2005a, 2005b, 2007).

In the central and western portions of the study area, at about 600 m a.s.l., biotite-rich and garnet-sillimanite gneisses gradually pass upward to migmatitic gneiss (Figures 4 and 5(b)). The migmatitic gneisses include biotite, garnet, sillimanite, quartz, plagioclase and minor K-feldspar and muscovite. The transition to migmatitic gneiss is marked, at the outcrop scale, by gradual reduction of mafic minerals to increasing sialic minerals. These rocks are poorly foliated and grey to brown in colour (Figure 5(b)).

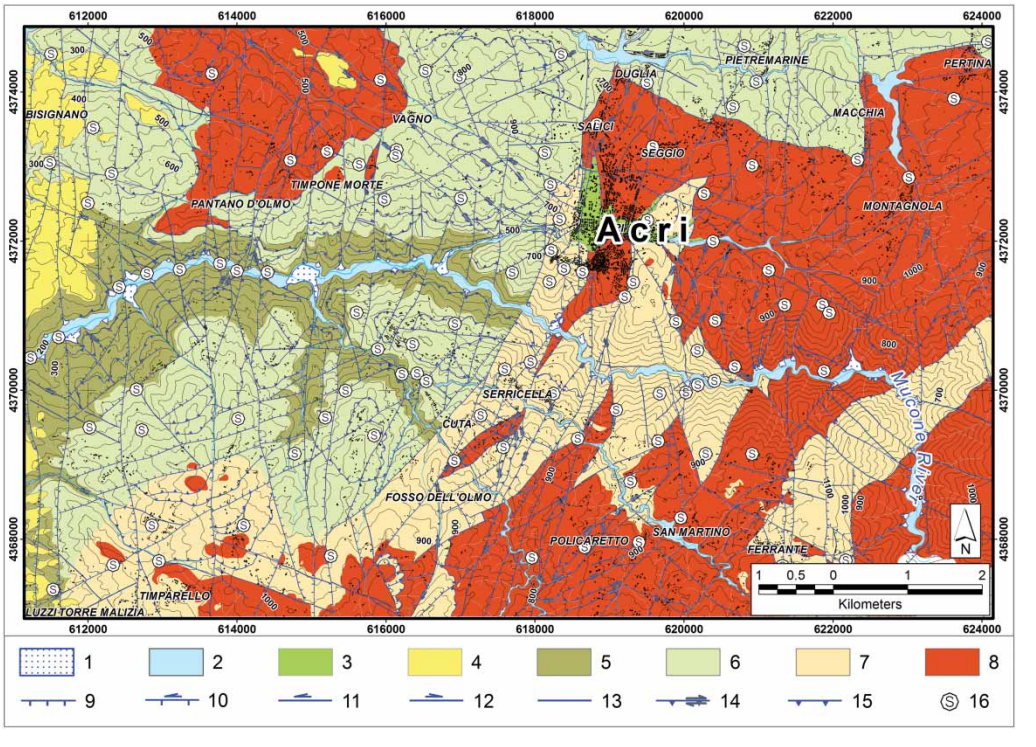

Figure 4. Geo-structural map of the study area. Legend: (1) alluvial and debris fan; (2) alluvial deposits; (3) fluvial conglomerates (Upper Pleistocene?); (4) matrix-supported conglomerates (Lower-Middle Pleistocene?); (5) biotite-garnet and sillimanite gneiss (Paleozoic); (6) biotite-sillimanite migmatitic gneiss occasionally with garnet (Paleozoic); (7) biotite-muscovite migmatitic gneiss (Paleozoic); (8) granitoid rocks with mainly tonalitic composition (Paleozoic); (9) normal fault; (10) left-lateral transcurrent fault reactivated as normal fault; (11) left-lateral transcurrent fault; (12) right-lateral transcurrent fault; (13) fault with undetermined kinematics; (14) high-angle transpressive thrust reactivated as normal fault; (15) low-angle thrust; and (16) mesostructural station.

In the south-eastern portion of map, along two zones oriented NE-SW, biotite-muscovite migmatitic gneiss are present (Figure 4). These rocks are characterized by alternating quartz-K feldspar and biotite-muscovite layers (Figure 5(c)). In the same area, close to the occurrence of plutonic rocks, the transition from the biotite-muscovite-rich migmatitic gneisses to granitoids is marked by the progressive reduction of mafic minerals and by the progressive lack of the foliation, with an increase of thin pegmatitic dykes.

The plutonic rocks prevail in the eastern portion of map (Figure 4); these rocks are mainly represented by tonalite (Figure 5(d)), passing locally to granodiorite with megacrysts of K-feldspar; sometimes they are intruded by pegmatite and aplite dykes. Mineralogy of plutonic rocks includes plagioclase, quartz, biotite, chlorite, muscovite and occasionally K-feldspar. Rocks are coarse grained and white in colour when they are unaltered, pink or reddish when intensely weathered.

In the western portions of the study area, unconformably overlying metamorphic rocks rests on the Pleistocene deposits (Figure 4). Early-to-middle Pleistocene sequences include brown-reddish basal conglomerates (Figure 5(e)), passing upward to interstratified conglomerates and brown-yellow sands. Upper Pleistocene? fluvial conglomerates, interbedded with coarse sand and thin mud, occur close to the Acri Village (Figures 4 and 5(f)).

Finally, Holocene alluvial deposits (Figure 5(g)) are present in the study area along the main rivers (Figure 4) and the piedmont portions of slopes. The last deposits are organized in alluvial and debris fans (Figure 5(h)).

From a tectonic perspective, a structural geological survey has been carried out. On the mapped tectonic structures (Figure 4) the geometry, trend and kinematics have been provided (Figures 6–8).

At macroscale, the three main tectonic structures exhibit N-S, NW-SE, NE-SW trends (Figure 4).

The N-S trending faults represent the most recent high-angle extensional faults, having fresh morphological evidence (Figures 4 and 6(a)). The N-S fault system includes a series of normal step faults, defining a system grading towards the west in the Crati River Basin. Fault planes show different slip-directions and pitch, sometimes superimposed (Figure 7(a)). Relative chronology of the kinematic indicators suggests that right transcurrent movements and oblique transpressive slip (Figures 6(b), 8(a and b)) postdates the last normal slip (Figure 8(c)).

The NW-SE fault system (Figures 4 and 6(c)) is well defined at macroscale and it as a widely distribution. The system is represented by sub-vertical, SW and NE dipping fault planes with superimposed kinematic indicators (Figure 7(b)). At the mesoscale, the NW-SE faults are characterized by left lateral-strike-slip movement (Figure 8(d–e)), even if overprinting of dip-slip displacements suggests reactivation as a normal fault during the last tectonic event (Figure 6(c)).

The NE-SW fault system is also widely represented along the study area (Figure 4), having overprinted kinematic indicators (Figure 7(c)). Inferred chronology for this fault system suggests a transcurrent or oblique-slip movement superimposed by dip-slip normal kinematics (Figure 6(d)).

The compressive tectonic structures (Figure 4), with poor morphological evidence, have been surveyed at the macro and mesoscale (Figures 6(e–h) and 8(f–h)). At the mesoscale, thrust faults have been subdivided into two main systems (Figure 7(d–e)).

The NW-SE thrusts have NE and SW dipping fault planes, which have a prevalent NE vergence. The planes with higher values of inclination and oblique pitch are related to the transpressional component of the system, while the subhorizontal plane is related to the more ancient structures, responsible for the duplex thrust stack development (Figure 7(d)).

Figure 5. Lithology outcropping in the study area: (a) biotite-garnet and sillimanite gneiss (Paleozoic); (b) biotite-sillimanite migmatitic gneiss occasionally with garnet (Paleozoic); (c) biotite-muscovite migmatitic gneiss (Paleozoic); (d) granitoid rocks with mainly tonalitic composition (Paleozoic); (e) matrix-supported conglomerates (Lower-Middle Pleistocene?); (f) fluvial conglomerates (Upper Pleistocene ?); (g) alluvial deposits; and (h) debris fan.

Figure 6. Examples of faults surveyed in the study area at the macro-scale: (a) N-S normal fault; (b) right-lateral transcurrent N-S fault with associated high-angle transpressive thrusts (flower structure); (c) left-lateral transcurrent NW-SE fault reactivated with normal kinematics; (d) NE-SW normal fault scarps; (e) medium-low angle thrust, displaced by N-S right-lateral transcurrent N-S fault, reactivated as normal fault; (f) detail of photo (e); (g) 'Acri-Caloveto' overthrust; and (h) low-angle tectonic contact linked to 'Acri-Caloveto' overthrust.

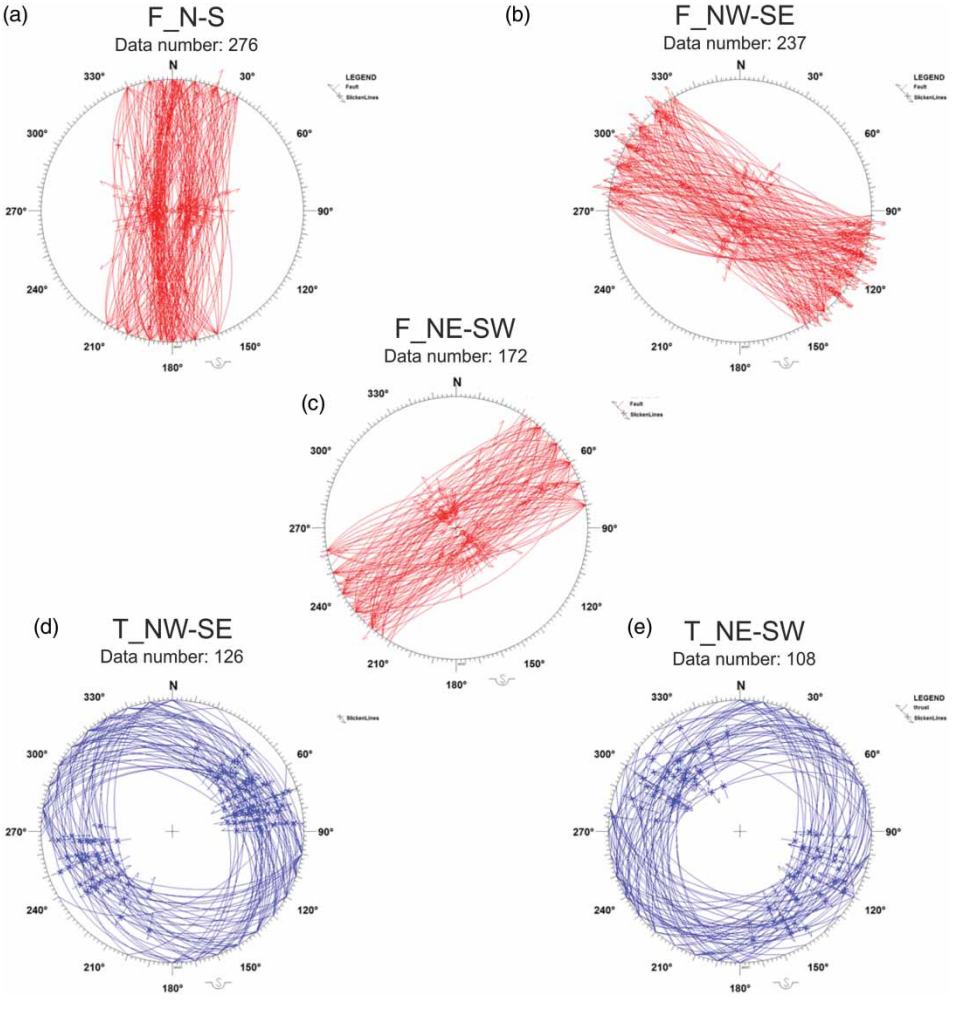

Figure 7. Lower hemisphere projection (Schmidt net) of the fault systems detected in the study area. For explanation see the text.

The second thrust system is represented by NE-SW trending, which have a ESE vergence and sub-horizontal to medium dip angle (Figures 7(e) and 8(f and g)). The thrust is related chronologically to the more ancient tectonic event of the study area, and mainly developed during accretionary processes involving the entire Sila Massif in the thrust belt (Figure 6(g and h)). In the field the NE-SW thrusts present a duplex structure, particularly when they involve the gneissic-granitoid complex (Figure 8(h)). Thick argillified fault gauges, are sometimes present along the major thrust planes (Figures 6(f) and 8(f)).

With regards to changes in the mechanical properties of the granitoid and gneissic rocks, five weathering classes, on the material and rock mass scale, have been distinguished in the field, from class II to class VI (Figures 9 and 10). The mapping of the weathering grade, shown in Figure 11, permits a general comprehensive overview of the effect, intensity and distribution of weathering classes (and therefore the weathering processes), linked to both the compositional heterogeneity of the outcropping crystalline-metamorphic rocks and the tectonic assemblage of the area.

Figure 8. Examples of meso-faults surveyed in the study area: (a) N-S transpressive faults; (b) double kinematics on a N-S fault plane (reverse and right-lateral); (c) last kinematics on the N-S fault plane; (d) NW-SE fault scarp; (e) left-lateral striae on the NW-SE fault plane of photo (d); (f) reverse fault; (g) ancient overthrust; and (h) ancient overthrusts displaced by a high-angle normal fault.

Slightly weathered rocks (class II) crop out only along deeply incised streams, particularly in the eastern portion of the Mucone River (Figure 11). The rock masses are slightly weathered (more than 70% of the outcrop) (Figure 9(a and b)); limited and isolated rock mass volumes, near the discontinuities constitute class III (moderately weathered rock). The rock material has the following characteristics: same colour as the fresh rock (class I) with discolouration only near the discontinuities; the original texture and microstructure of the fresh rock are perfectly preserved; the strength is comparable to that of the fresh rock (hard rock); they make a ringing sound when it is struck by hammer; Schmidt hammer rebound values is more than 50.

Moderately weathered rocks (class III) outcrop predominantly along the lower portions of the slopes and also along stream incisions (e.g. Mucone River and tributary streams) (Figure 11). The rock masses are moderately weathered (more than 70% of the outcrop) (Figure 9(c and d)); limited and isolated rock mass volumes can be composed of highly or slightly weathered rock (respectively classes IV and II). The rock material has the following characteristics: pervasively discoloured, but locally the colour of the fresh rock can be present; the original texture and microstructure of the fresh rock are well preserved; the strength is comparable to that of the fresh rock (hard rock); the rock makes an intermediate sound when it is struck by the hammer; large fragments can be broken if it is struck by the head of the hammer; the point of geological hammer can produce a scratch on the surface of rock; Schmidt hammer rebound values of 25–50.

Highly weathered rocks (class IV) outcrop mainly along the middle and upper portions of the slopes and along the lower portions of minor stream incisions (Figure 11). The rock masses are highly weathered (more than 70% of the outcrop) (Figure 9(e and f)); limited and isolated rock mass volumes can be composed of moderately or completely weathered rock (respectively classes III and V). The rock material has the following characteristics: completely discoloured; the original texture and microstructure of the fresh rock are still preserved; the strength is substantially reduced (weak rock); they make an intermediate dull sound when struck by the hammer; large pieces are easily broken if they are struck by the hammer and do not slake in water; the point of geological hammer indents the rock superficially; the knife edge produces a scratch on the surface of rock; Schmidt hammer rebound values of 10–25.

Completely weathered rocks (class V) are present in elevated areas, mainly above of 700 m a.s.l. (Figure 11). The rock masses are completely weathered (more than 70% of the outcrop) (Figure 9(g and h)); limited and isolated rock mass volumes can be composed of highly weathered rock or residual soil (respectively classes IV and VI). The rock material has the following characteristics: completely discoloured; the original texture and microstructure of the fresh rock are present in relict form; soil like behaviour; large pieces can be broken by hand or crumbled by finger pressure into constituent grains and slake in water; the point of geological pick indents the rock deeply; the knife edge easily carves the surface of rock; gravel and sand fractions are prevalent; Schmidt hammer rebound values of 0–15.

Weathered rocks are locally covered by residual, colluvial and detrital soils (grade VI) (Figure 10). Residual soils, with not surveyable thickness (at the scale of map), are mainly present in elevated areas (as relicts of paleosurfaces), and present predominantly sand and silts fractions (Figure 10(a and b)). Colluvial soils are mainly present in morphological hollows, where the thickness can reach several metres (Figure 10(c)); colluvial soils are formed by sandy-silty chaotic deposits, including moderately to highly weathered centimetric rock fragments and subordinately organic fragments. Slope debris and landslide debris, metres to decametres thick, are distributed along the slopes and at the valley bottom. The volumes are composed of detrital-colluvial soils and represented by disorganized deposits

Figure 9. Examples of weathering classes surveyed in the study area and effects of weathering increase upward from slightly weathered rocks (class II) to completely weathered rocks (class V): (a) gneiss class II; (b) granitoid class II; (c) gneiss class III; (d) granitoid class III; (e) gneiss class IV; (f) granitoid class IV; (g) gneiss class V; and (h) granitoid class V.

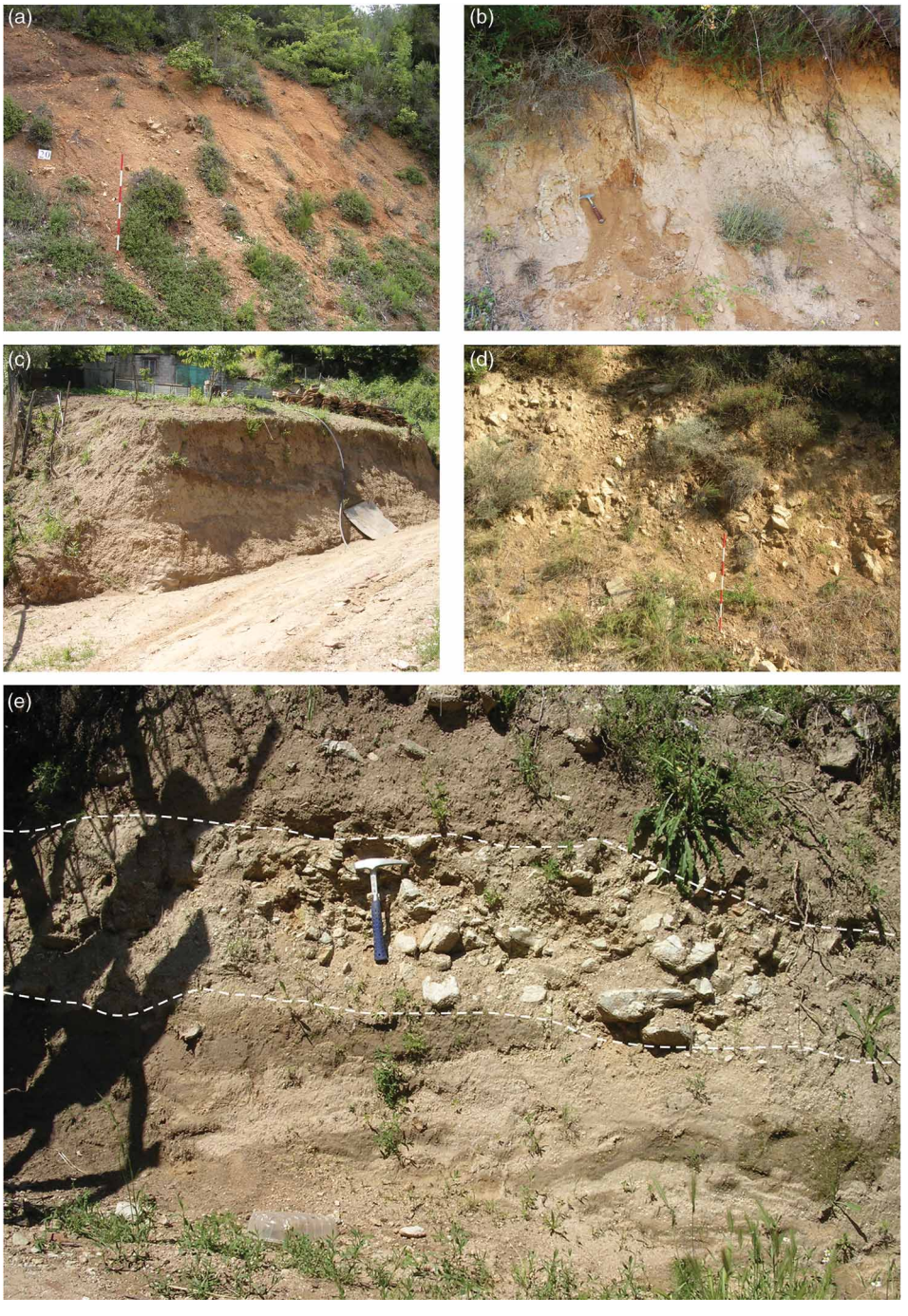

Figure 10. Examples of terrains (in situ weathered soils and transported soils) grouped in class VI: (a) residual soils from gneiss; (b) residual soils from granitoid; (c) colluvial soils; (d) detrital deposits; and (e) alternating colluvial and detrital deposits.

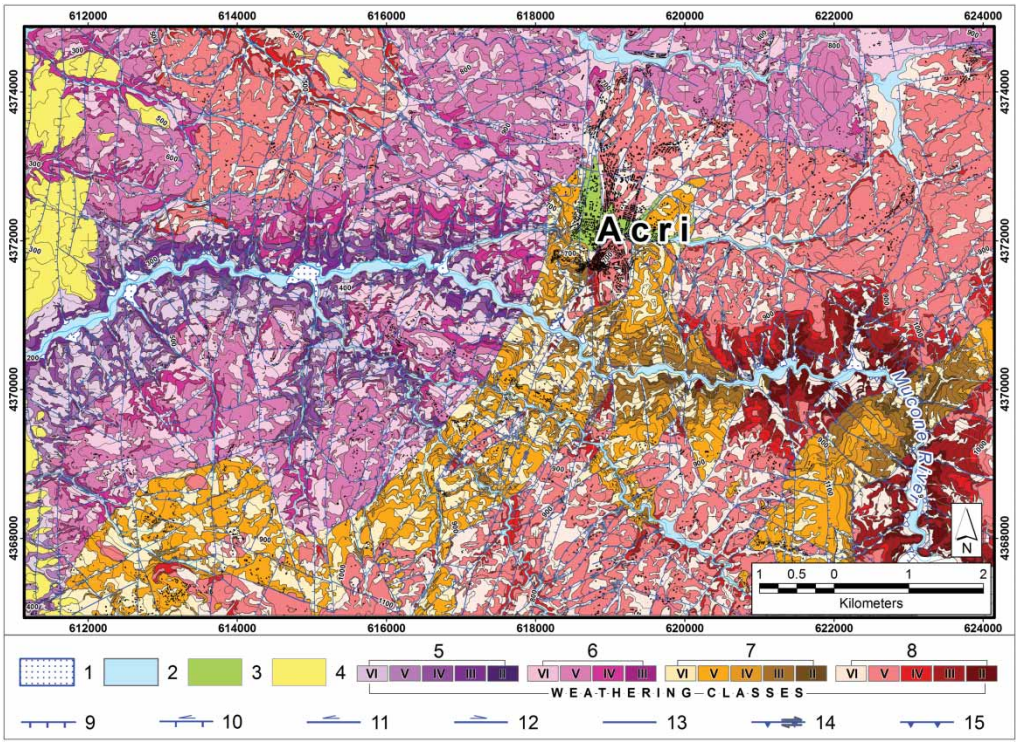

Figure 11. Weathering grade and geotectonic map of the study area. Legend: (1) alluvial and debris fan; (2) alluvial deposits; (3) fluvial conglomerates; (4) matrix-supported conglomerates; (5) weathering classes of the biotite-garnet and sillimanite gneiss; (6) weathering classes of the biotite-sillimanite migmatitic gneiss; (7) weathering classes of the biotite-muscovite migmatitic gneiss; (8) weathering classes of the granitoid rocks; (9) normal fault; (10) left-lateral transcurrent fault reactivated as normal fault; (11) left-lateral transcurrent fault; (12) right-lateral transcurrent fault; (13) fault with undetermined kinematics; (14) high-angle transpressive thrust reactivated as normal fault; and (15) low-angle thrust.

(Figure 10(d)); they are formed by sand and gravel including moderately to highly weathered decimetric rock fragments and subordinately organic fragments. Moreover, alternating detrital and colluvial deposits are grouped in class VI (Figure 10(e)).

5. Conclusions

The field surveys conducted in the West-Central side of the Mucone River basin, have provided a detailed picture of the geological-structural features and the spatial distribution of weathering classes in the outcropping crystalline rocks. The study methodology has tested the weathering-grade survey and mapping procedure in the specific granitoid and gneissic rocks. In particular, it has been shown to be a reliable and rapid technique, which uses simple qualitative and semi-quantitative index tests, for medium-large-scale studies and investigations.

The large-scale geo-structural and weathering-grade map represents a useful tool for territorial planning and engineering-geological and environmental purposes, providing a fundamental contribution to the assessment of landslide and soil erosion hazards.

Software

The weathering-grade map and related layout (Figures 1, 2, 4, and 11) were produced using Esri ArcGIS 10.0. Corel Draw X6 was used for compiling Figures 3, 5, 6–10. Mesostructural data reported in Figure 7 were produced using Daisy 3 (Salvini, 2011).

Acknowledgements

This work was carried out under the Commessa TA.P05.012 'Tipizzazione di eventi naturali e antropici ad elevato impatto sociale ed economico' of the CNR — Department 'Scienze del sistema Terra e Tecnologie per l'Ambiente'. Data and information were collected during the research related to the PhD Thesis of Borrelli (2008).

The authors thank Professor Francesco Dramis, Dr. Massimo Conforti, and Dr. Thomas Pingel for providing constructive comments, which have contributed to improvement of the manuscript and map.

References

Barone, M., Dominici, R., Muto, F., & Critelli, S. (2008). Detrital modes in a late Miocene wedge-top basin, northeastern Calabria, Italy: Compositional record of wedge-top partitioning. *Journal of Sedimentary Research*, *78*, 693–711.

Baynes, F. J., Dearman, W. R., & Irfan, T. Y. (1978). Practical assessment of grade in a weathered granite. *Bulletin of the International Association of Engineering Geology*, *18*, 101–109.

Bell, D. H., & Pettinga, J. R. (1985). Engineering geology and subdivision planning in New Zealand. *Engineering Geology*, *22*, 45–59.

Borrelli, L. (2008). *Categorie di frane ed elementi caratteristici nei profili di alterazione* (Unpublished doctoral dissertation). University of Calabria.

Borrelli, L., Greco, R., & Gullà, G. (2007). Weathering grade of rock masses as a predisposing factor to slope instabilities: Reconnaissance and control procedures. *Geomorphology*, *87*, 158–175.

Borrelli, L., Cofone, G., & Gullà, G. (2012a). Procedura speditiva per la redazione di una carta del grado di alterazione a scala regionale. *Rendiconti online della Società Geologica Italiana*, *21*, 528–530.

Borrelli, L., Perri, F., Critelli, S., & Gullà, G. (2012b). Minero-petrographical features of weathering profiles in Calabria, southern Italy. *Catena*, *92*, 196–207.

Borrelli, L., Perri, F., Critelli, S., & Gullà, G. (2014). Characterization of granitoid and gneissic weathering profiles of the Mucone River basin (Calabria, southern Italy). *Catena*, *113*, 325–340.

Calcaterra, D., & Parise, M. (2005). Landslide types and their relationships with weathering in a Calabrian basin, southern Italy. *Bullettin of Engineering Geology and the Environment*, *64*, 193–207.

Calcaterra, D., & Parise, M. (2010). Weathering in the crystalline rocks of Calabria, Italy, and relationships to landslides. In D. Calcaterra & M. Parise (Eds.), *Weathering as a predisposing factor to slope movements* (pp. 105–130). Geological Society of London, 23. Engineering Geology Special Publication.

Cascini, L., Critelli, S., Di Nocera, S., Gullà, G., & Matano, F. (1992). Grado di alterazione e franosità negli gneiss del Massiccio silano: L'area di S. Pietro in Guarano (CS). *Geologia Applicata e Idrogeologia*, *27*, 49–76.

Conforti, M., Muto, F., Rago, V., & Critelli, S. (2014). Landslide inventory map of North-eastern Calabria (South Italy). *Journal of Maps*, *110*, 90–102.

Corbi, F., Fubelli, G., Lucà, F., Muto, F., Pelle, T., Robustelli, G., … Dramis, F. (2009). Vertical movements in the Ionian margin of the Sila Massif (Calabria, Italy). *Bollettino Società Geologica Italiana*, *128*, 731–738.

Critelli, S., Muto, F., Tripodi, V., & Perri, F. (2013). Link between thrust tectonics and sedimentation processes of stratigraphic sequences from the southern Apennines foreland basin system, Italy. *Rendiconti Online della Società Geologica Italiana*, *25*, 21–42.

Dearman, W. R. (1974). Presentation of information on engineering geological maps and plans. *Quarterly Journal of Engineering Geology and Hydrogeology*, *7*, 317–320.

Dearman, W. R. (1991). *Engineering geology mapping*. Oxford: Butterworth and Heinemann.

Dearman, W. R., & Eyles, N. (1982). An engineering geological map of the soils and rocks of the United Kingdom. *Bulletin of the International Association of Engineering Geology*, *25*, 3–18.

Dearman, W. R., & Matula, M. (1976). Environmental aspects of engineering geological mapping. *Bulletin of the International Association of Engineering Geology*, *14*, 141–146.

Fabbricatore, D., Robustelli, G., & Muto, F. (2014). Facies analysis and depositional architecture of shelf-type deltas in the Crati Basin (Calabrian Arc, south Italy). *Italian Journal of Geosciences*, *133*, 131–148.

Faccini, F., Robbiano, A., Roccati, A., & Angelini, S. (2012). Engineering geological map of the Chiavari city area (Liguria, Italy). *Journal of Maps*, *8*, 41–47.

Garfi, G., Bruno, D., Calcaterra, D., & Parise, M. (2007). Fan morphodynamics and slope instability in the Mucone River basin (Sila Massif, southern Italy): Significance of weathering and role of land use changes. *Catena*, *69*, 181–196.

Geological Society Engineering Group Working Party. (1995). The description and classification of weathered rocks for engineering purposes. *Quarterly Journal of Engineering Geology and Hydrogeology*, *28*, 207–242.

Geotechnical Control Office. (1988). *Guide to rock and soil descriptions*. Hong Kong: Civil Engineering Services Department.

Grman, D., Waniekova, D., Petro, L., & Polascinova, E. (2002). *Engineering geological maps of the Tibreg region. Geologica Carpathica*. Special Issue, 53, Proceedings of XVII Congress of Carpathian-Balkan Geological Association, Bratislava, September, 1–4, 2002.

Gullà, G., & Matano, F. (1997). *Surveys of weathering profile on gneiss cutslopes in Northern Calabria, Italy.* Proceedings of the International Symposium on engineering Geology and the Environment, IAEG, Athens, 133–138.

Guzzetta, G. (1974). Ancient tropical weathering in Calabria. *Nature*, *251*, 302–303.

International Association of Engineering Geology. (1976). *Engineering geological maps: A guide to their preparation*. Paris: Unesco Press.

International Association of Engineering Geology. (1981). Rock and soil description for engineering geological mapping. *Bulletin of the International Association of Engineering Geology*, *24*, 235–274.

Irfan, T. Y., & Dearman, W. R. (1978). Engineering classification and index properties of a weathered granite. *Bulletin of the International Association of Engineering Geology*, *17*, 79–90.

Lanzafame, G., & Tortorici, L. (1981). La Tettonica recente della Valle del Fiume Crati (Calabria). *Geografia Fisica e Dinamica Quaternaria*, *4*, 11–21.

Le Pera, E., Arribas, J., Critelli, S., & Tortosa, A. (2001a). The effects of source rocks and chemical weathering on the petrogenesis of siliciclastic sand from the Neto River (Calabria, Italy): Implications for provenance studies. *Sedimentology*, *48*, 357–377.

Le Pera, E., Critelli, S., & Sorriso-Valvo, M. (2001b). Weathering of gneiss in Calabria, Southern Italy. *Catena*, *42*, 1–15.

Lozinska-Stepien, H. (1979). Engineering geological maps at a scale 1:25 000 for regional planning purposes. *Bulletin of Engineering Geology and the Environment*, *19*, 69–72.

Maharaj, R. J. (1995). Engineering-geological mapping of tropical soils for land-use planning and geotechnical purposes: A case study from Jamaica, West Indies. *Engineering Geology*, *40*, 243–286.

Malomo, S., Olorunniwo, M. A., & Ogunsanwo, O. (1983). Engineering geological mapping in terrains of tropical weathering – An example from Abuja, Nigeria. *Engineering Geology*, *19*, 133–148.

Matano, F., & Di Nocera, S. (1999). Weathering patterns in the Sila Massif (northern Calabria, Italy). *Italian Journal of Quaternary Sciences*, *12*, 141–148.

Messina, A., Russo, S., Borghi, A., Colonna, V., Compagnoni, R., Caggianelli, A., … Piccarreta, G. (1994). Il Massiccio della Sila Settore settentrionale dell'Arco Calabro-Peloritano. *Bollettino della Società Geologica Italiana*, *113*, 539–586.

Molin, P., Pazzaglia, F. J., & Dramis, F. (2004). Geomorphic expression of active tectonics in a rapidly deforming forearc, Sila Massif, Calabria, southern Italy. *American Journal of Science*, *304*, 559–589.

Perri, F., Borrelli, L., Gullà, G., & Critelli, S. (2014). Chemical and minero-petrographic features of Plio-Pleistocene fine-grained sediments in Calabria, southern Italy. *Italian Journal of Geosciences*, *133*, 101–115.

Perri, F., Critelli, S., Dominici, R., Muto, F., Tripodi, V., & Ceramicola, S. (2012). Provenance and accommodation pathways of late quaternary sediments in the deep-water northern Ionian Basin, southern Italy, in quantitative models in sediment generation (Eds. Critelli S., von Eynatten H., Ingersoll R.V., Weltje G.). *Sedimentary Geology Special Issue*, *280*, 244–259.

Salvini, F. (2011). *Daisy 3, the structural data integrated analyzer. Free distribution by e-mailing to daisy@uniroma3.it*. Roma: Dipartimento di Scienze Geologiche, Università di 'Roma Tre'.

Scarciglia, F., Le Pera, E., & Critelli, S. (2005a). Weathering and pedogenesis in the Sila Grande Massif (Calabria, South Italy): From field scale to micromorphology. *Catena*, *61*, 1–29.

Scarciglia, F., Le Pera, E., & Critelli, S. (2007). The onset of sedimentary cycle in a mid-latitude upland environment: Weathering, pedogenesis and geomorphic processes on plutonic rocks (Sila Massif, Calabria). In J. Arribas, S. Critelli, & M. Johnsson (Eds.), *Sedimentary provenance: Petrographic and geochemical perspectives* (pp. 149–166). Geological Society of America Special Paper 420.

Scarciglia, F., Le Pera, E., Vecchio, G., & Critelli, S. (2005b). The interplay of geomorphic processes and soil development in un upland environment, Calabria, South Italy. *Geomorphology*, *64*, 1–23.

Spina, V., Tondi, E., & Mazzoli, S. (2011). Complex basin development in a wrench-dominated back-arc area: Tectonic evolution of the Crati Basin, Calabria, Italy. *Journal of Geodynamics*, *51*, 90–109.

Tansi, C., Muto, F., Critelli, S., & Iovine, G. (2007). Neogene-quaternary strike-slip tectonics in the central Calabrian Arc (Southern Italy). *Journal of Geodynamics*, *43*, 393–414.

Tortorici, L., Monaco, C., Tansi, C., & Cocina, O. (1995). Recent and active tectonics in the Calabrian arc (Southern Italy). *Tectonophysics*, *234*, 37–55.

Van Dijk, J. P., Bello, M., Brancaleoni, G. P., Cantarella, G., Costa, V., Frixa, A., … Zerilli, A. (2000). A regional structural model for the northern sector of the Calabria Arc (Southern Italy). *Tectonophysics*, *324*, 267–320.

Zuquette, L. V., Pejon, O. J., & dos Santos Collares, J. Q. (2004). Engineering geological mapping developed in the Fortaleza metropolitan region, State of Ceara, Brazil. *Engineering Geology*, *71*, 227–253.